Article ID: 1000-324X(2020)04-0482-09 **DOI:** 10.15541/jim20190154

Removal of Volatile Organic Compounds Driven by Platinum Supported on Amorphous Phosphated Titanium Oxide

HUANG Xieyi[1,2], WANG Peng[2,3], YIN Guoheng[1], ZHANG Shaoning[1], ZHAO Wei[1], WANG Dong[1], BI Qingyuan[1], HUANG Fuqiang[1,3,4]

(1. State Key Laboratory of High Performance Ceramics and Superfine Microstructure, Shanghai Institute of Ceramics, Chinese Academy of Sciences, Shanghai 200050, China; 2. University of Chinese Academy of Sciences, Beijing 100049, China; 3. School of Physical Science and Technology, ShanghaiTech University, Shanghai 200031, China; 4. State Key Laboratory of Rare Earth Materials Chemistry and Applications, College of Chemistry and Molecular Engineering, Peking University, Beijing 100871, China)

Abstract: Development of high efficiency catalyst is the key factor to catalytic combustion of volatile organic compounds (VOCs). Herein, amorphous mesoporous phosphated TiO_2 (ATO-P) with high specific surface area supported platinum catalyst was successfully fabricated. P-dopant can increase the surface area (up to 278.9 $m^2 \cdot g^{-1}$) of ATO-P, which is 21 times higher than that of pristine TiO_2, and make the amorphous titanium oxide structure. The supported Pt catalyst with amorphous mesoporous feature shows impressive performance and excellent thermostability for VOCs oxidation. The Pt/ATO-P catalyst exhibits outstanding catalytic efficiency, the T_{50} and T_{90} (temperatures required for achieving conversions of 50% and 90%) are respectively 130 ℃ and 140 ℃, for toluene oxidation under high gas hourly space velocity (GHSV) of 36000 $mL \cdot h^{-1} \cdot g^{-1}$ and toluene concentration of 10000 $mL \cdot m^{-3}$. The performance is superior to the reference Pt/TiO_2 and comparable with the state-of-the-art catalysts. These findings can make a significant contribution on the new applications of amorphous mesoporous phosphated materials in VOCs removal.

Key words: amorphous mesoporous structure; phosphated TiO_2; Pt nanoparticle; toluene oxidation; VOCs removal

Volatile organic compounds (VOCs), like toluene, benzene, esters and hydrocarbons, are emitted from various industrial sources which can cause serious environmental pollution and health problems[1−2]. Toluene, one kind of toxic and strong carcinogenic chemical, is frequently used in making paints, adhesives, rubbers, and leather tanning processes because of its excellent ability to dissolve organic substances[3-4]. However, toluene is difficult to degrade due to its stable structure[5]. Several techniques, such as physical and chemical adsorption, photocatalytic and catalytic oxidation methods, are widely used for the combustion of VOCs[6-7]. Among them, catalytic oxidation is regarded as a promising approach owing to its high efficiency and convenient operating conditions[8].

Researches on catalysts for toluene oxidation have been conducted, including noble metal and metal oxides catalysts[9-10]. Due to the significant reduction on activation energy during the catalytic oxidation process, noble metal based catalysts, such as Pt, Pd, Au, Rh, and Ir have shown impressive performance in toluene removal[11-13]. It was found that supported Pt catalysts showed the best catalytic performance compared with other noble metals[14-15]. It should be pointed out that the supports play an important role in the catalytic reaction processes[16-18]. Many works have focused on the metal-support interaction by studying the catalytic properties of TiO_2, Al_2O_3, ZrO_2, and ZnO supported Au nanoparticles[19], and the shape effect of Pt/CeO_2 catalysts[10]. Nevertheless, most supports suffer from low specific surface area and few active sites, which are crucial for the overall catalytic activity.

Received date: 2019-04-12; **Revised date:** 2019-05-24
Foundation item: National Key Research and Development Program of China (2016YFB0901600); National Natural Science Foundation of China (21872166); Science & Technology Commission of Shanghai (16ZR1440400, 16JC1401700); The Key Research Program of Chinese Academy of Sciences (QYZDJ-SSW-JSC013 and KGZD-EW-T06)
Biography: Huang Xieyi (1994–), male, Master candidate. E-mail: huangxieyi@student.sic.ac.cn
黄谢意(1994–), 男, 硕士研究生. E-mail: huangxieyi@student.sic.ac.cn
Corresponding author: BI Qingyuan, associate professor. E-mail: biqingyuan@mail.sic.ac.cn;
HUANG Fuqiang, professor. E-mail: huangfq@mail.sic.ac.cn
毕庆元, 副研究员. E-mail: huangfq@mail.sic.ac.cn; 黄富强, 研究员. E-mail: huangfq@mail.sic.ac.cn

Due to high specific surface area and variable valence, amorphous materials have attracted increasing interests in VOCs oxidation. And the numerous defects in amorphous structures can offer large quantities of oxygen vacancies, which are beneficial for the adsorption of oxygen and organic molecules. Lee, *et al*[20]. reported that carbon black supported amorphous MnO_x is highly efficient for oxygen involved reaction. Wang, *et al*[21] found that amorphous MnO_x modified Co_3O_4 can enhance the catalytic activity for the VOCs oxidation. It was demonstrated that the amorphous structure of bimetallic Pd-Pt/CeO_2-Al_2O_3-TiO_2 could provide more vacancies and active sites for catalytic combustion[22]. Therefore, the amorphous catalysts show a tremendous potential in practical catalytic reactions. However, it is still a challenge to develop highly active and robust catalysts based on the amorphous materials for the oxidation of VOCs.

Herein, we demonstrate an efficient Pt/ATO-P catalyst for the catalytic removal of VOCs under high gas hourly space velocity (GHSV) and high substrate concentration. It should be pointed out that incorporating phosphorus into the framework of TiO_2 is a widely applied strategy for obtaining amorphous mesoporous feature[23-24]. And the P element can stabilize the TiO_2 framework and significantly increase the specific surface area[24].

1 Experimental

1.1 Preparation of sample

1.1.1 Preparation of support

All reagents were of analytical grade and were used without any purification. 3 mL of tetrabutyl titanate was dissolved in 30 mL of ethanol at room temperature, which was marked as solution A. Then 0.125 mL of phosphoric acid (H_3PO_4) was subsequently dropwisely added into solution A with stirring to form a homogenous mixture, and kept stirring for 24 h. The obtained white solid products were separated by centrifuge, and washed by deionized water and ethanol several times, followed by freeze drying overnight. The as-prepared products were calcined at 400 ℃ in air for 4 h at a heating rate of 5 ℃·min^{-1}.

1.1.2 Preparation of catalyst

The ATO-P supported platinum (Pt/ATO-P) sample was prepared *via* impregnation method. A desired amount of ATO-P was transferred into aqueous solution containing appropriate amount of chloroplatinic acid (H_2PtCl_4). Subsequently, the samples were impregnated at room temperature for 12 h. After drying out the H_2O at 80 ℃, the samples were treated at 350 ℃ for 2 h with a H_2/Ar mixture (5/95, *V*/*V*).

1.2 Characterization

XRD characterization of the samples was carried out on a German Bruker D8 Advance X-ray diffractometer (XRD) using the Ni-filtered Cu Kα radiation at 40 kV and 40 mA. Nitrogen adsorption-desorption isotherms were measured at –196 ℃ on a Micromeritics ASAP 2460 analyzer. Samples were degassed at 120 ℃ for 24 h prior to the measurement. The specific surface area of the samples was calculated using the Brunauer–Emmett–Teller (BET) method with the adsorption data at the relative pressure (p/p_0) range of 0.05–0.2. The total pore volumes were estimated at p/p_0=0.99. The pore size distribution (PSD) curves were calculated from the adsorption branch using Barrett-Joyner-Halenda (BJH) model. The prepared materials were pressed into tablets with KBr powder and then detected by FT-IR (Perkin Elmer, USA) in the scanning range from 400 to 4000 cm^{-1}. SEM images were obtained by Hitachi-S4800. A JEOL 2011 microscope operating at 200 kV equipped with an EDX unit (Si(Li) detector) was used for the transmission electron microscope (TEM) and high resolution transmission electron microscope (HRTEM) investigations. The samples for TEM testing were prepared by dispersing the powder in ethanol and applying a drop of highly dilute suspension on carbon-coated grids. XPS data were recorded with a Perkin Elmer PHI 5000 C system equipped with a hemispherical electron energy analyzer. The spectrometer was operated at 15 kV and 20 mA, and a magnesium anode (Mg Kα, hv=1253.6 eV) was used. The C1s line (284.6 eV) was used as the reference to calibrate the binding energies (BE). TG measurements were conducted on a Netzsch STA 449C TG-DSC thermoanalyzer. The flow rate of the carrier gas (air) was 30 mL·min^{-1}. The temperature was raised from room temperature to 800 ℃ at a ramp rate of 10 ℃·min^{-1}. Prior to H_2-TPR test, the sample (100 mg) was pretreated at 200 ℃ for 2 h and cooled to 50 ℃ in the flowing He. TPR experiment was carried out in 5vol% H_2/He flowing at 30 mL·min^{-1}, with a ramping rate of 5 ℃·min^{-1} to a final temperature of *ca.* 800 ℃. The signal was monitored using a TCD detector.

1.3 Catalytic activity test

The catalytic activity of samples was evaluated in a continued-flow fixed-bed quartz reactor with 50 mg catalyst. Toluene was introduced into the reactor with bubbling toluene solution in ice bath with pure air. The concentration of toluene was about 10^4 mL·m^{-3}, and the flow rate was kept at 30 mL·min^{-1} by a mass controller, equivalent to a gas hour space velocity (GHSV) of 36000 mL·h^{-1}·g^{-1}. After steady operation for 100 min, the activity of the catalyst was tested. Toluene concen-

tration was detected by a gas chromatograph equipped with a flame ionization detector. The toluene conversion ($X_{toluene}$) was calculated according to the equation:

$$X_{toluene} = (C_{in}–C_{out})/C_{in}·100\% \quad (1)$$

where C_{in} and C_{out} are the inlet and outlet toluene concentrations, respectively.

2 Results and discussion

2.1 Physicochemical properties of ATO-P support

Fig. 1 displays the schematic diagram of amorphous ATO-P prepared *via* facile co-precipitation. XRD patterns of ATO-P and TiO_2 are shown in Fig. 2. All diffraction peaks of basic TiO_2 sample are indexed to anatase phase (JCPDS 21-1276). Interestingly, there is no TiO_2 crystal phase observed for ATO-P sample (Fig. 2), suggesting that ATO-P sample is typically amorphous and phosphorus dopant can markedly restrain the crystallization of anatase[25−26].

According to the TGA-DSC thermograms (Fig. 3), a thermal decomposition of ATO-P took place in the temperature range of 20−900 ℃. The first DSC peak at 30−80 ℃ is due to the release of physical adsorbed water. When all the water is released, Ti−OH and HPO_4^{2-} groups start to condense[27]. These processes occur simultaneously in the temperature range of 100−220 ℃ (1.927% of weight loss) and 220−516 ℃ (0.7% of weight loss), resulting in an overlap of the TG data. There is no further weight loss up to 516 ℃. The DSC curve shows two exothermic peaks at 704 and 781 ℃, corresponding to a two-step exothermic transformation of ATO-P into a crystalline phase.

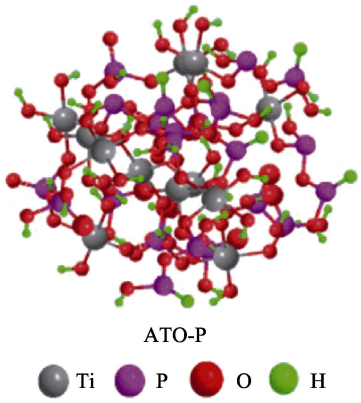

Fig. 1 Structure of amorphous ATO-P prepared *via* facile co-precipitation

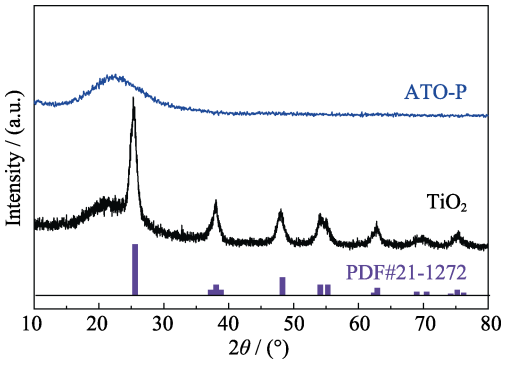

Fig. 2 XRD patterns of TiO_2 and ATO-P samples

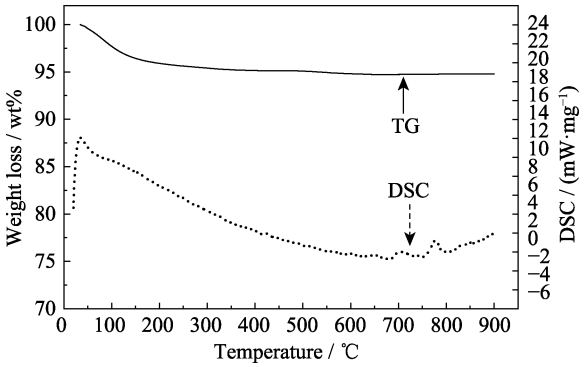

Fig. 3 TG (solid line) and DSC (dashed line) curves for ATO-P

Fig. 4(a,b) show the SEM images of ATO-P. The ATO-P nanoparticles are homogeneously dispersed with the particle size of ~20 nm, and the sizes are similar to that of TiO_2 (Fig. S1(a)). HRTEM was employed to characterize the nanostructure of samples. No porous structure is observed in the HRTEM image of TiO_2 (Fig. S1(b)), while various porous structure is shown in ATO-P (Fig. 4(c)). Moreover, the pores of ATO-P are uniform, and the average diameter is around 10 nm. EDS elemental mappings indicate that the P element homogeneously distributes in ATO-P (Fig. 4(d)). It is found that H_3PO_4 owns unique effects for synthesizing amorphous mesoporous phosphated TiO_2[28-29].

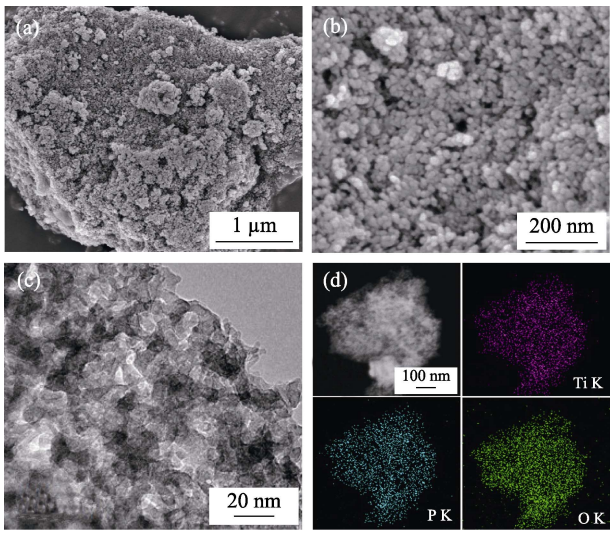

Fig. 4 SEM (a, b) and HRTEM (c) images, and EDS elemental mapping (d) of ATO-P

As shown in Fig. 5, the obtained ATO-P sample shows a characteristic type-IV isotherm with clear hysteresis loop locates at the p/p_0 range of 0.45−1.0, showing the existence of a large amount of mesopore. Notably, the specific surface area of 278.9 $m^2 \cdot g^{-1}$ for ATO-P is 21 times higher than that of pristine TiO_2. The pore diameters of ATO-P center around 10 nm (Fig. 5 and Table 1), which is consistent with HRTEM result (Fig. 4(c)).

The results of EDX are listed in Table 1. The actual P concentration is much less than the initial addition amount of H_3PO_4, suggesting that partial H_3PO_4 is leached during the preparation process.

FT-IR spectra of TiO_2 and ATO-P samples are depicted in Fig. 6. The wide absorption bands around 3440 and 1620 cm^{-1} are attributed to the surface adsorbed water and/or hydroxyl groups[30-31]. The bands at 1100 cm^{-1} are ascribed to the stretching vibration of Ti−O−P species, which are absent in TiO_2. The weak bands at 610 cm^{-1} are due to the vibration of Ti−O−Ti bond[22]. Compared with TiO_2, a weak peak appears in series ATO-P, which may result from the incorporating effect of phosphorus dopant. There is no distinct peak over the range of 700−800 cm^{-1} (Fig. 6), indicating the absence of P−O−P groups in the amorphous mesoporous phosphated TiO_2. Therefore, the P element is incorporated into the frameworks of ATO-P by forming Ti−O−P bonds[24].

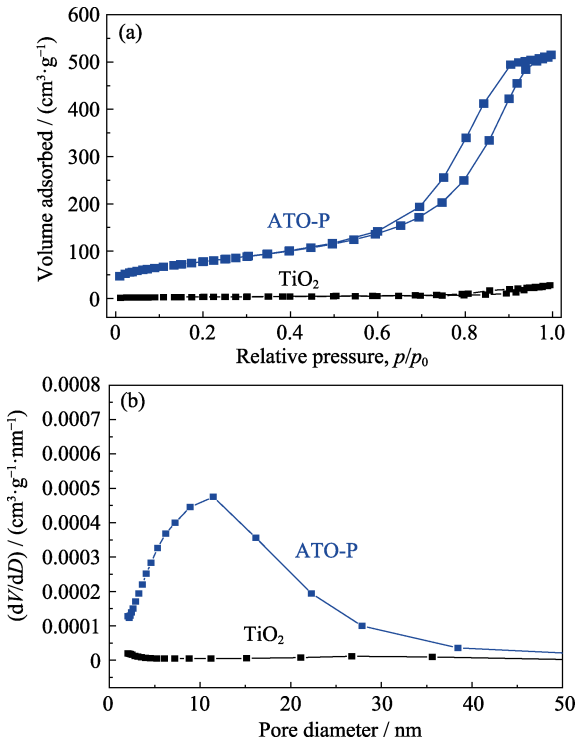

Fig. 5　N_2 adsorption-desorption isotherms (a) and pore size distributions (b) of ATO-P and TiO_2

Table 1　Textural properties and elemental compositions of TiO_2 and ATO-P samples

Catalyst	BET surface area /($m^2 \cdot g^{-1}$)	Pore volume /($cm^3 \cdot g^{-1}$)	Pore size /nm	Elemental composition /wt%[a]		
				P	Ti	O
TiO_2	10.9	0.04	15.7	–	60.0	40.0
ATO-P	278.9	0.80	11.4	19.2	32.1	48.7

[a] Weight fraction (wt%) are determined by EDX analysis

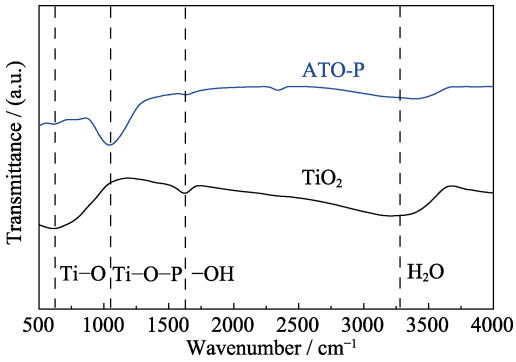

Fig. 6　FT-IR spectra of TiO_2 and ATO-P

As shown in Fig. 7(a), the full XPS spectra indicate the existence of P in ATO-P. High-resolution XPS spectra of P 2p, Ti 2p and O 1s are depicted in Fig. 7(b−d). The peak of P 2p of ATO-P is at 134.0 eV, suggesting that phosphorus in ATO-P gives a pentavalent oxidation state of P^{5+}. No peak observed at 128.6 eV, which is the characteristic binding energy of P2p in TiP, indicating the absence of Ti−P bonds in ATO-P samples. As depicted in Fig. 7(c), the peaks of $Ti2p_{3/2}$ and $Ti2p_{1/2}$ in ATO-P show remarkable blue-shift owing to the incorporation effect of phosphorus element. Fig. 7(d) shows the XPS spectra of O1s signals of TiO_2 and ATO-P. The single peak at 529.5 eV is corresponded to the oxygen in Ti−O bond of TiO_2. However, the O1s spectrum of ATO-P contains two peaks at 531.4 and 532.9 eV, which are contributed to Ti−O−P and O−H bond, respectively[32-33].

2.2　Physicochemical properties of Pt/ATO-P catalysts

Fig. 8(a) shows that the Pt nanoparticles are well dispersed over the ATO-P support, and the size is relatively uniform with the average parameter of (1.8±0.3) nm (insert in Fig. 8(a)). Fig. 8(b) and S2 demonstrate a *d*-spacing of 0.23 nm, attributed to the (111) plane of the highly crystalline Pt nanostructure. Furthermore, the actual Pt content was also confirmed by inductively coulped plasma atomic emission spectra (ICP-AES). The mass loadings of Pt in Pt/TiO_2 and Pt/ATO-P catalysts are 0.90 and 0.92, respectively, which are close to the nominal composition of 1wt%.

Fig. 8(c) shows the XRD patterns of Pt/ATO-P and Pt/TiO_2 catalysts. The amorphous structure is still remained

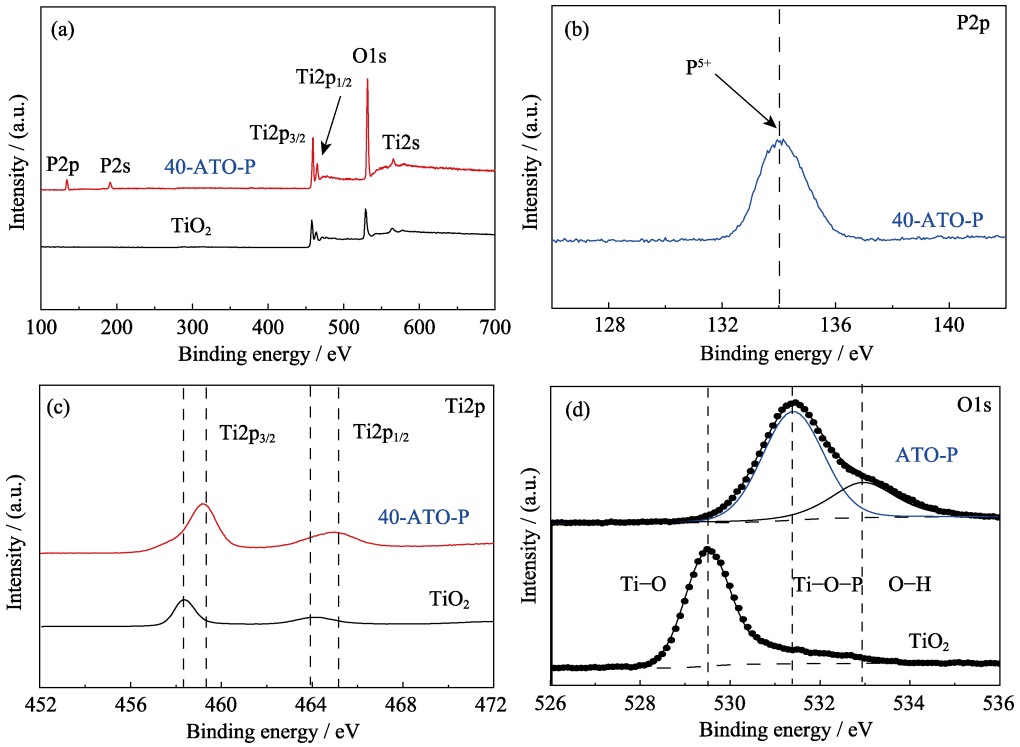

Fig. 7 Full XPS spectra (a) of TiO_2 and ATO-P; High-resolution XPS P2p (b), Ti2p (c), and O1s (d) of TiO_2 and ATO-P

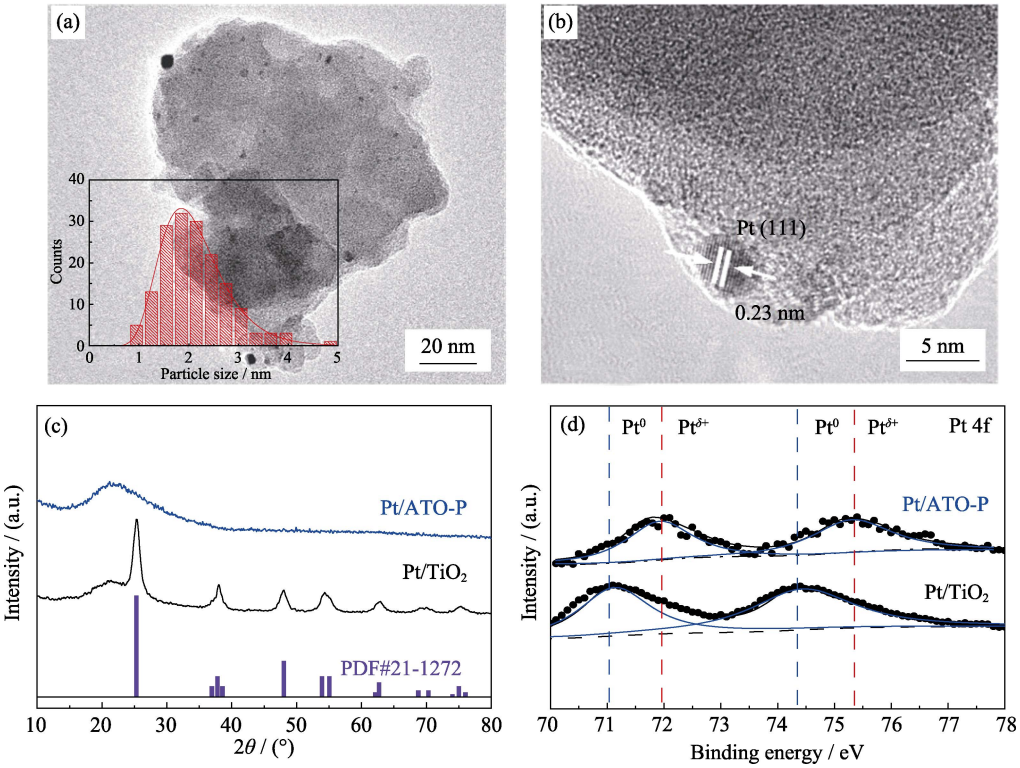

Fig. 8 TEM (a) and HRTEM (b) images of Pt/ATO-P with insert in (a) indicating the particle size distribution of Pt nanoparticles, XRD patterns (c) and XPS Pt4f (d) of Pt/ATO-P

for Pt/ATO-P sample. However, no diffraction pattern of Pt nanoparticles is observed, indicating that the Pt nanoparticles are quite small and/or the Pt species are highly dispersed on the ATO-P surface. These results are well consistent with the HRTEM data above mentioned in Fig. 8(a, b).

The results of XPS analysis of Pt/ATO-P and Pt/TiO_2 samples are depicted in Fig. 8(d). It is known that the positions of $Pt4f_{7/2}$ binding energy at 71.1, 72.4, and 74.2 eV are attributed to Pt^0, Pt^{2+}, and Pt^{4+} species, respec-

tively[34]. Similiar XPS profiles are rendered as the indication of a mixture of various valence states for Pt species over the small Pt nanoparticles. The exisence of $Pt^{\delta+}$ species reflects the strong metal-support interaction (Pt−ATO-P), especially the prominent electronic interaction between active Pt and underlying phosphated TiO_2 support[35]. This is probably due to the changes of the metal-support interaction by doping phosphorus atoms which can make an obvious effect on Ti−O−P frameworks.

The H_2-TPR profiles depicted in Fig. S3 show that there are two H_2-consumption peaks at low and high temperature attributed to weak and strong interaction of Pt and supports, respectively[36]. Notably, two reduction peaks of Pt/ATO-P catalyst at 78 and 601 ℃ show stronger intensity than that of Pt/TiO_2 at 72 and 433 ℃, indicating strong Pt-support interaction for Pt/ATO-P. These results are consistent with the XPS data.

2.3 Removal of VOCs by Pt/ATO-P catalysts

The catalytic efficiencies are depicted in Fig. 9. It is clearly observed that reaction temperature can enhance the performance of Pt/ATO-P catalyst. The T_{50} and T_{90} are widely used to evaluate the catalytic performance[37]. As shown in Fig. 9(a), Pt/ATO-P shows the excellent catalytic activity. T_{50} and T_{90} values for toluene combustion are 130 and 140 ℃, which are much lower than those of Pt/TiO_2 with T_{50} and T_{90} of 160 and 190 ℃, respectively. Combined with the above XPS data (Fig. 8(d)), it can be concluded that the existance of phosphorus component plays an important role in electronic structure of the active Pt species underlying amorphous mesoporous ATO-P support and thus the catalytic oxidation removal of toluene over Pt/ATO-P catalyst.

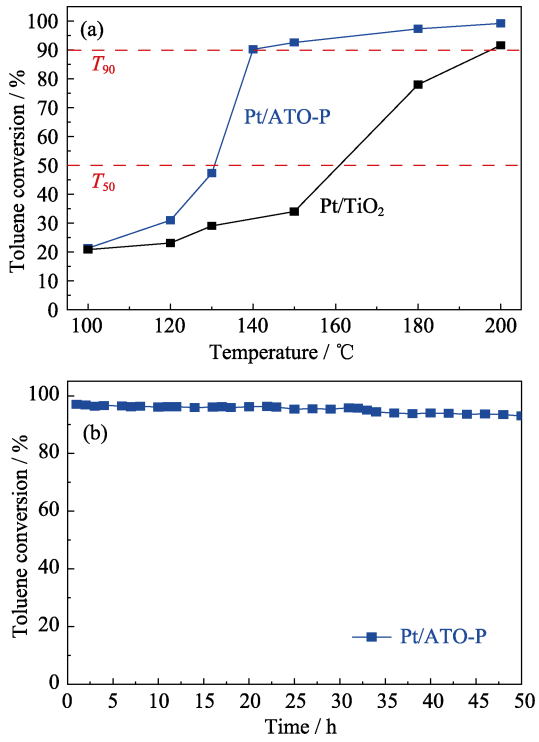

Fig. 9　Toluene conversion (a) of 1wt% Pt/ATO-P with respect to reaction temperature, and thermal stability (b) of Pt/ATO-P at 180 ℃

It is well known that noble metal loading significantly affects the catalytic behavior for many reactions. Pt/ATO-P catalysts with different Pt loadings were examined, and the results are depicted in Fig. 10. Compared with 0.5wt% and 2wt%, the Pt loading of 1wt% shows better performance (lower T_{50} and T_{90}) for toluene oxidation. The low catalytic activity of 0.5 wt% Pt/ATO-P results from low density of active platinum nanoparticles anchoring on the surface of ATO-P support. For the Pt/ATO-P catalyst with Pt loading up to 2wt%, larger size of Pt nanopartices (~5 nm) can be obtained (Fig. S4). Larger Pt particles can not only decrease the dispersion of Pt species[38], but also lead to a weaker metal-support (Pt/ATO-P) interactions, thus resulting in the poor activity.

Stability is critical for the catalysts on the practical application. 1wt% Pt/ATO-P exhibits excellent thermal stability for toluene oxidation over a 50-h period on stream at 180 ℃ without visible loss of activity, as shown in Fig. 9(b). The toluene conversion remains a high level of 95.4% at the end of reaction process and maintains near full selectivity to final products of CO_2 and H_2O. The excellent stability of Pt/ATO-P catalyst is attributed to the unique geometric structure of crystalline Pt nanoparticles and amorphous mesoporous phosphated TiO_2 with prominent electronic interaction. For the used 1wt% Pt/ATO-P, TEM measurement and XPS analysis (Fig. S5 and Fig. S6) demonstrate no significant change on the morphology, average size of Pt nanoparticles, and the chemical oxidation state of active Pt species. These results suggest the robustness of Pt/ATO-P catalyst for toluene oxidation removal under a relatively mild thermal process.

Given the superb thermocatalytic performance for

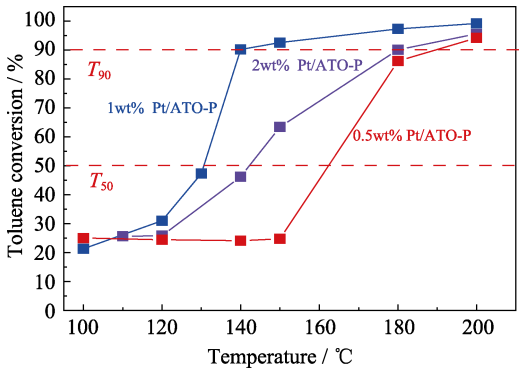

Fig. 10　Toluene conversion over Pt/ATO-P catalysts with different Pt loadings

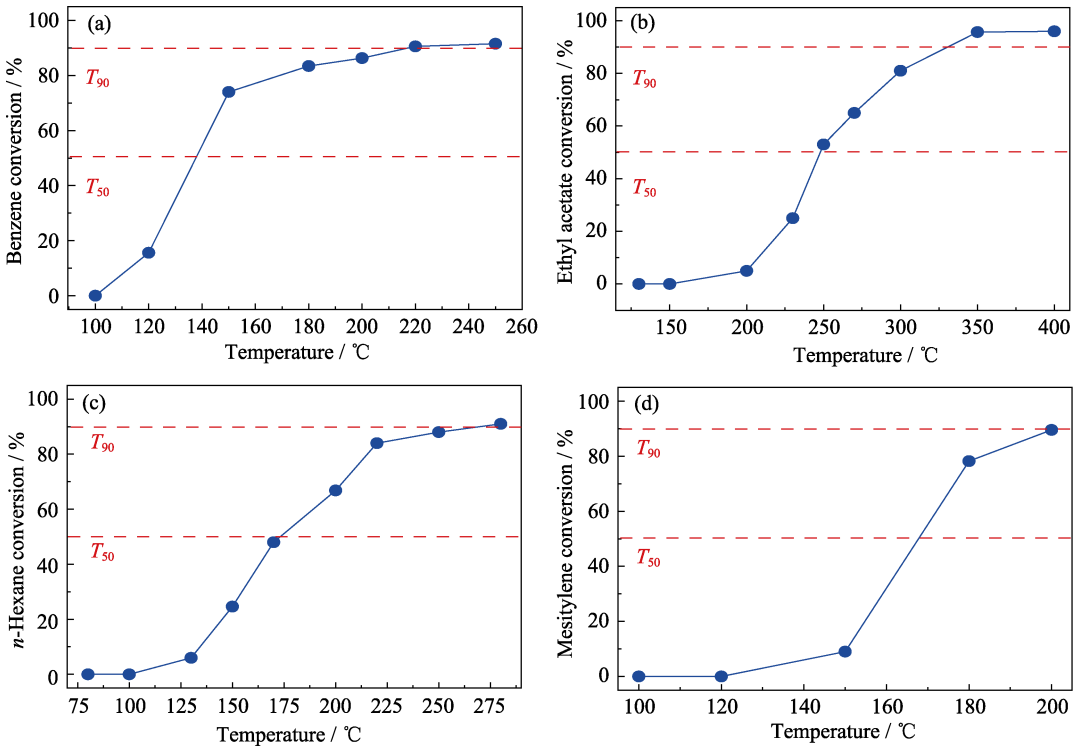

Fig. 11 Catalytic activity of Pt/ATO-P for the conversion of benzene (a), ethyl acetate (b), *n*-hexane (c), and mesitylene (d) with respect to reaction temperature

1wt% Pt/ATO-P catalyst toward toluene oxidation, we were curious to examine whether the engineered material would also catalyze the removal of a class of VOCs, especially the complete oxidation of benzene, *n*-hexane, ethyl acetate, and mesitylene. As depicted in Fig. 11, the T_{90} values for the catalytic oxidation of benzene, ethyl acetate, *n*-hexane, and mesitylene are 216, 331, 271, and 200 ℃, respectively. Notably, high temperature is required for ethyl acetate conversion at 90% due to its strong structural stability[39-40]. These results show a broad scope toward catalytic combustion involving troublesome organic compounds over Pt/ATO-P and indicate that the Pt/ATO-P catalysts can provide a new insight for the oxidation of VOCs.

3 Conclusions

In summary, we successfully fabricated the amorphous mesoporous phosphated TiO_2 supported platinum catalysts for efficient removal of volatile organic compounds. The electronic modifications of supported Pt nanoparticles for the underlying amorphous ATO-P material and Pt loading for the whole catalyst were systematically investigated. The phosphorus dopant played an important role for stabilizing the inflated Ti−O−P frameworks as well as the electronic structure of Pt species. Compared with pristine TiO_2, ATO-P with high specific surface area showed significant enhancement for Pt/ATO-P samples for catalytic overall oxidation of toluene under practical conditions. The performance of the engineered Pt/ATO-P for toluene combustion was superior to the reference Pt/TiO_2 and comparable with the state-of-the-art catalysts. Additionally, Pt/ATO-P catalyst exhibited excellent stability for toluene oxidation removal under a relatively mild thermal process and could be potentially applied in a broad scope of VOCs. The present work is expected to make a significant contribution on the new application of amorphous mesoporous phosphated material in VOCs removal.

Supporting Materials

Supporting Materials related to this article can be found at https://doi.org/10.15541/jim20190154.

References:

[1] XIE S H, LIU Y X, DENG J G, *et al*. Insights into the active sites of ordered mesoporous cobalt oxide catalysts for the total oxidation of *o*-xylene. *Journal of Catalysis*, 2017, **352:** 282–292.

[2] GENUINO H C, DHARMARATHNA S, NJAGI E C, *et al*. Gas-phase total oxidation of benzene, toluene, ethylbenzene, and xylenes using shape-selective manganese oxide and copper manganese oxide catalysts. *Journal of Physical Chemistry C*, 2012, **116(22):** 12066–12078.

[3] SIHAIB Z, PULEO F, GARCIA-VARGAS J M, *et al*. Manganese oxide-based catalysts for toluene oxidation. *Applied Catalysis B: Environmental*, 2017, **209(15):** 689–700.

[4] ROKICIŃSKA A, DROZDEK M, DUDEK B, *et al*. Cobalt-containing BEA zeolite for catalytic combustion of toluene. *Applied Catalysis B: Environmental*, 2017, **212:** 59–67.

[5] SANTOS V P, PEREIRA M F R, ÓRFÃO J J M, *et al*. The role of lattice oxygen on the activity of manganese oxides towards the oxidation of volatile organic compounds. *Applied Catalysis B: Environmental*, 2010, **99(1/2):** 353–363.

[6] ŠULIGOJ A, ŠTANGAR U L, RISTIĆ A, *et al*. TiO_2-SiO_2 films from organic-free colloidal TiO_2 anatase nanoparticles as photocatalyst for removal of volatile organic compounds from indoor air. *Applied Catalysis B: Environmental*, 2016, **184:** 119–131.

[7] QIAN X F, YUE D T, TIAN Z Y, *et al*. Carbon quantum dots decorated Bi_2WO_6 nanocomposite with enhanced photocatalytic oxidation activity for VOCs. *Applied Catalysis B: Environmental*, 2016, **193:** 16–21.

[8] CHEN J, CHEN X, XU W J, *et al*. Homogeneous introduction of CeO_y into MnO_x-based catalyst for oxidation of aromatic VOCs. *Applied Catalysis B: Environmental*, 2018, **224:** 825–835.

[9] YANG H G, DENG J G, LIU Y X, *et al*. Preparation and catalytic performance of Ag, Au, Pd or Pt nanoparticles supported on 3DOM CeO_2-Al_2O_3 for toluene oxidation. *Journal of Molecular Catalysis A: Chemical*, 2016, **414:** 9–18.

[10] PENG R S, SUN X B, LI S J, *et al*. Shape effect of Pt/CeO_2 catalysts on the catalytic oxidation of toluene. *Chemical Engineering Journal*, 2016, **306:** 1234–1246.

[11] ALGHAMDI A O, JEDIDI A, AZIZ S G, *et al*. Theoretical insights into dehydrogenative chemisorption of alkylaromatics on Pt(100) and Ni(100). *Journal of Catalysis*, 2018, **363:** 197–203.

[12] ZHANG Z X, JIANG Z, SHANGGUAN W F. Low-temperature catalysis for VOCs removal in technology and application: a state-of-the-art review. *Catalysis Today*, 2016, **264:** 270–278.

[13] XIE S H, LIU Y X, DENG J G, *et al*. Effect of transition metal doping on the catalytic performance of Au-Pd/3DOM Mn_2O_3 for the oxidation of methane and *o*-xylene. *Applied Catalysis B: Environmental*, 2017, **206:** 221–232.

[14] SANTOS V P, CARABINEIRO S A C, TAVARES P B, *et al*. Oxidation of CO, ethanol and toluene over TiO_2 supported noble metal catalysts. *Applied Catalysis B: Environmental*, 2010, **99(1/2):** 198–205.

[15] FU X R, LIU Y, YAO W Y, *et al*. One-step synthesis of bimetallic Pt-Pd/MCM-41 mesoporous materials with superior catalytic performance for toluene oxidation. *Catalysis Communications*, 2016, **83:** 22–26.

[16] YIN G H, HUANG X Y, CHEN T Y, *et al*. Hydrogenated blue titania for efficient solar to chemical conversions: preparation, characterization, and reaction mechanism of CO_2 reduction. *ACS Catalysis*, 2018, **8(2):** 1009–1017.

[17] WU D W, ZHANG Q L, LIN T, *et al*. Effect of Fe on the selective catalytic reduction of NO by NH_3 at low temperature over Mn/CeO_2-TiO_2 catalyst. *Journal of Inorganic Materials*, 2012, **27(5):** 495–500.

[18] YU W W, ZHANG Q H, SHI G Y, *et al*. Preparation of Pt-loaded TiO_2 nanotubes/nanocrystals composite photocatalysts and their photocatalytic properties. *Journal of Inorganic Materials*, 2011, **26(7):** 747–752.

[19] COMOTTI M, LI W C, SPLIETHOFF B, *et al*. Support effect in high activity gold catalysts for CO oxidation. *Journal of the American Chemical Society*, 2006, **128(3):** 917–924.

[20] LEE J S, PARK G S, LEE H I, *et al*. Ketjenblack carbon supported amorphous manganese oxides nanowires as highly efficient electrocatalyst for oxygen reduction reaction in alkaline solutions. *Nano Letters*, 2011, **11(12):** 5362–5366.

[21] ZHENG Y L, WANG W Z, JIANG D, *et al*. Amorphous MnO_x modified Co_3O_4 for formaldehyde oxidation: improved low-temperature catalytic and photothermocatalytic activity. *Chemical Engineering Journal*, 2016, **284:** 21–27.

[22] GUO Y Y, ZHANG S, MU W T, *et al*. Methanol total oxidation as model reaction for the effects of different Pd content on Pd-Pt/CeO_2-Al_2O_3-TiO_2 catalysts. *Molecular Catalysis*, 2017, **429:** 18–26.

[23] CLEARFIELD A, THAKUR D S. Zirconium and titanium phosphates as catalysts: a review. *Applied Catalysis*, 1986, **26:** 1–26.

[24] YU J C, ZHANG L Z, ZHENG Z, *et al*. Synthesis and characterization of phosphated mesoporous titanium dioxide with high photocatalytic activity. *Chemistry of Materials*, 2003, **15(11):** 2280–2286.

[25] KŐRÖSI L, OSZKÓ A, GALBÁCS G, *et al*. Structural properties and photocatalytic behaviour of phosphate-modified nanocrystalline titania films. *Applied Catalysis B: Environmental*, 2007, **77(1/2):** 175–183.

[26] KÖRÖSI L, PAPP S, BERTÓTI I, *et al*. Surface and bulk composition, structure, and photocatalytic activity of phosphate-modified TiO_2. *Chemistry of Materials*, 2007, **19(19):** 4811–4819.

[27] MASLOVA M V, RUSANOVA D, NAYDENOV V, *et al*. Synthesis, characterization, and sorption properties of amorphous titanium phosphate and silica-modified titanium phosphates. *Inorganic Chemistry*, 2008, **47(23):** 11351–11360.

[28] ZHU Y L, ZHOU W, SUNARSO J, *et al*. Phosphorus-doped perovskite oxide as highly efficient water oxidation electrocatalyst in alkaline solution. *Advanced Functional Materials*, 2016, **26(32):** 5862–5872.

[29] HEO Y W, PARK S J, IP K, *et al*. Transport properties of phosphorus-doped ZnO thin films. *Applied Physics Letters*, 2003, **83(6):** 1128–1130.

[30] YIN G H, BI Q Y, ZHAO W, *et al*. Efficient conversion of CO_2 to methane photocatalyzed by conductive black titania. *ChemCatChem*, 2017, **9(23):** 4389–4396.

[31] PLUMEJEAU S, RIVALLIN M, BROSILLON S, *et al*. The reductive dehydration of cellulose by solid/gas reaction with $TiCl_4$ at low temperature: a cheap, simple, and green process for preparing anatase nanoplates and TiO_2/C composites. *Chemistry-A European Journal*, 2016, **22(48):** 17262–17268.

[32] REN T Z, YUAN Z Y, AZIOUNE A, *et al*. Tailoring the porous hierarchy of titanium phosphates. *Langmuir*, 2006, **22(8):** 3886–3894.

[33] YOSHIDA H, YAZAWA Y, HATTORI T. Effects of support and additive on oxidation state and activity of Pt catalyst in propane combustion. *Catalysis Today*, 2003, **87(1-4):** 19–28.

[34] TIERNAN M J, FINLAYSON O E. Effects of ceria on the combustion activity and surface properties of Pt/Al_2O_3 catalysts. *Applied Catalysis B: Environmental*, 1998, **19(1):** 23–25.

[35] LYKHACH Y, FAISAL F, SKÁLA T, *et al*. Interplay between the metal-support interaction and stability in Pt/Co_3O_4 (111) model catalysts. *Journal of Materials Chemistry A*, 2018, **6:** 23078–23086.

[36] ZHANG C B, HE H, TANAKA KI. Catalytic performance and mechanism of a Pt/TiO_2 catalyst for the oxidation of formaldehyde at room temperature. *Applied Catalysis B: Environmental*, 2006, **65:** 37–43.

[37] RAHMANI F, HAGHIGHI M, ESTIFAEE P. Synthesis and characterization of Pt/Al_2O_3-CeO_2 nanocatalyst used for toluene abatement from waste gas streams at low temperature: conventional *vs.* plasma-ultrasound hybrid synthesis methods. *Microporous and Mesoporous Materials*, 2014, **185(1):** 213–223.

[38] CHEN C Y, CHEN F, ZHANG L, *et al*. Importance of platinum

particle size for complete oxidation of toluene over Pt/ZSM-5 catalysts. *Chemical Communications*, 2015, **51:** 5936–5938.
[39] LI S M, HAO Q L, ZHAO R Z, *et al*. Highly efficient catalytic removal of ethyl acetate over Ce/Zr promoted copper/ZSM-5 catalysts. *Chemical Engineering Journal*, 2016, **285:** 536–543.
[40] CARABINEIRO S A C, CHEN X, MARTYNYUK O, *et al*. Gold supported on metal oxides for volatile organic compounds total oxidation. *Catalysis Today*, 2015, **244:** 103–114.

掺磷非晶氧化钛负载铂用于高效催化氧化挥发性有机化合物

黄谢意[1,2], 王 鹏[2,3], 尹国恒[1], 张绍宁[1], 赵 伟[1], 王 东[1], 毕庆员[1], 黄富强[1,3,4]

(1. 中国科学院 上海硅酸盐研究所, 高性能陶瓷和超微结构国家重点实验室, 上海 200050; 2. 中国科学院大学, 北京 100049; 3. 上海科技大学 物理科学与技术学院, 上海 200050; 4. 北京大学 化学与分子工程学院, 稀土材料化学及应用国家重点实验室, 北京 100871)

摘 要: 高活性催化剂是挥发性有机化合物(VOCs)催化氧化消除的关键因素。本研究通过简单的共沉淀法成功制备了具有高比表面积的非晶介孔磷掺杂氧化钛负载铂催化剂(Pt/ATO-P)。通过 P 掺杂, 既可获得非晶介孔结构, 又可获得高 ATO-P 比表面积(可达 278.9 $m^2 \cdot g^{-1}$)。非晶介孔 Pt/ATO-P 催化剂显示出优异的 VOCs 催化氧化性能和良好的热稳定性。Pt/ATO-P 样品在空速为 36000 $mL \cdot h^{-1} \cdot g^{-1}$、甲苯浓度为 10000 $mL \cdot m^{-3}$ 的反应条件下, 对甲苯催化氧化的 T_{50} 和 T_{90}(实现 50%和 90%转化率所需的温度)分别为 130 ℃和 140 ℃, 明显优于无磷催化剂 Pt/TiO_2。这些发现可以为拓展非晶介孔磷化材料在环境净化和能源转化等领域的应用提供重要参考。

关 键 词: 非晶介孔材料; 磷掺杂非晶氧化钛; 铂纳米颗粒; 甲苯催化氧化; VOCs 消除

中图分类号: O782 **文献标识码:** A

Supporting Materials:

Removal of Volatile Organic Compounds Driven by Platinum Supported on Amorphous Phosphated Titanium Oxide

HUANG Xie-Yi[1,2], WANG Peng[2,3], YIN Guo-Heng[1], ZHANG Shao-Ning[1],
ZHAO Wei[1], WANG Dong[1], BI Qing-Yuan[1], HUANG Fu-Qiang[1,3,4]

(1. State Key Laboratory of High Performance Ceramics and Superfine Microstructure, Shanghai Institute of Ceramics, Chinese Academy of Sciences, Shanghai 200050, China; 2. University of Chinese Academy of Sciences, Beijing 100049, China; 3. School of Physical Science and Technology, ShanghaiTech University, Shanghai 200031, China; 4. State Key Laboratory of Rare Earth Materials Chemistry and Applications, College of Chemistry and Molecular Engineering, Peking University, Beijing 100871, China)

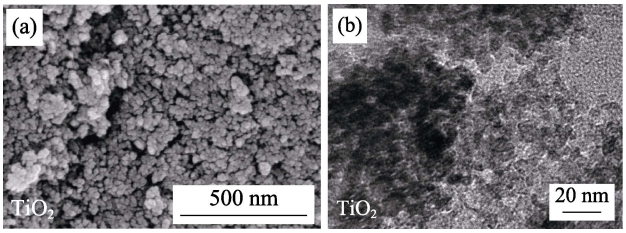

Fig. S1　SEM (a) and HRTEM (b) images of TiO_2

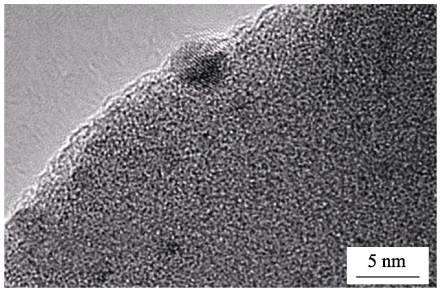

Fig. S2　HRTEM image of Pt/ATO-P

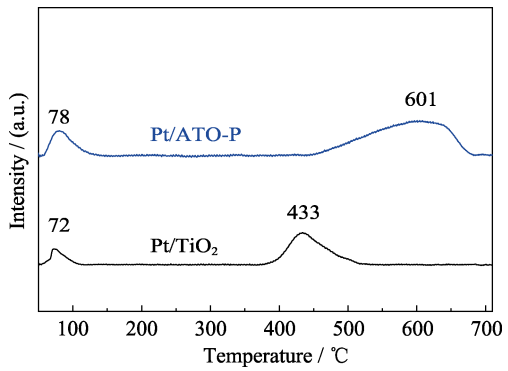

Fig. S3　H_2-TPR profiles of Pt/TiO_2 and Pt/ATO-P samples

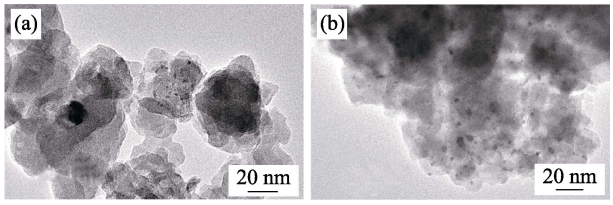

Fig. S4　TEM images of 0.5wt% Pt/ATO-P (a) and 2wt% Pt/ATO-P (b)

For the catalyst with low loading of 0.5wt%, there are few Pt nanoparticles in the ATO-P supports. By contract, the Pt particles are larger than that with loading of 1wt% when the loading up to 2wt%

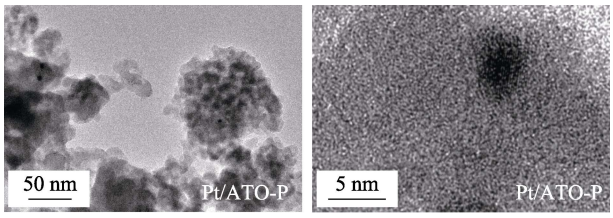

Fig. S5　TEM (a) and HRTEM (b) images of the used Pt/ATO-P catalyst

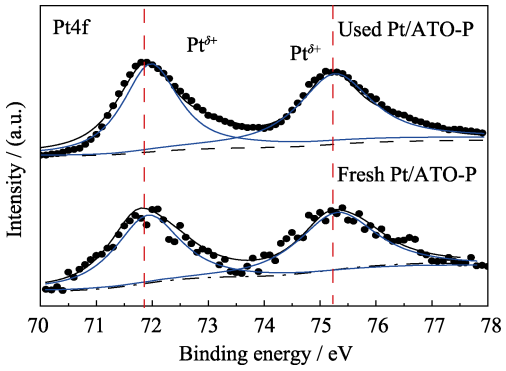

Fig. S6　XPS Pt 4f spectra of the fresh and the used Pt/ATO-P catalysts